Inorganic Chemistry

Article

pubs.acs.org/IC

Three New Alkaline Beryllium Borates $LiBeBO_3$, $Li_6Be_3B_4O_{12}$, and $Li_8Be_5B_6O_{18}$ in the Ternary Phase Diagrams $Li_2O-BeO-B_2O_3$

Shichao Wang, Ning Ye,* and Guohong Zou

Key Laboratory of Optoelectronic Materials Chemistry and Physics, Fujian Institute of Research on the Structure of Matter, Chinese Academy of Sciences, Fuzhou, Fujian, 350002, P. R. China

Supporting Information

ABSTRACT: The phase diagram in the $Li_2O-BeO-B_2O_3$ system has been systematically investigated by the methods of visual polythermal analysis, spontaneous crystallization, and X-ray diffraction. Three new alkaline beryllium borates, namely, $LiBeBO_3$, $Li_6Be_3B_4O_{12}$, and $Li_8Be_5B_6O_{18}$, were synthesized with molten fluxes based on $Li_2O-B_2O_3$ solvent in this system. All of the materials are centrosymmetric. The similarity of the fundamental building block of the title compounds has been compared. Thermal analysis and powder XRD studies were applied to determine phase relation and their incongruent melting behavior. The UV−vis diffuse reflectance spectroscopy demonstrated that the UV cutoff edges of the aforementioned materials are all below 200 nm.

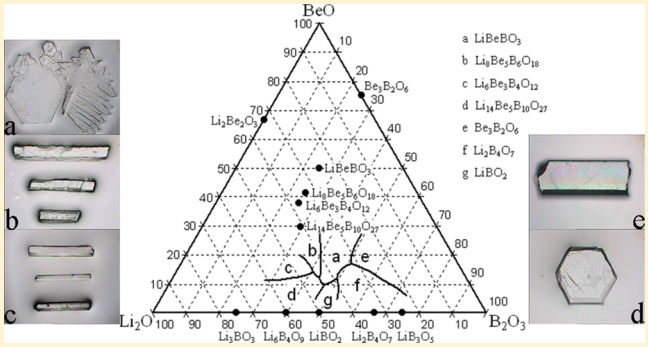

INTRODUCTION

With the developments in lithography, patterning, information storage, micromachining, laser spectroscopy, biomedical research, and sensor technology, the need for ultraviolet (UV) optical materials has become increasingly urgent over the past decade. At present, the materials generally used for these applications consist mainly of inorganic crystals based on fluoride,[1] such as LiF, MgF_2, CaF_2, and BaF_2, which can be made into high transparency and low loss optical windows, prisms, and lenses. Borate crystals also play an important role in the field of UV optics due to their unique UV transparency and high damage threshold. For example, α-BaB_2O_4[2] crystal can be used as an excellent birefringent crystal for linear optics in optical polarizing components and walk-off beam splitters, especially for high power operations in the UV wave band. Certainly, the most important application of borate crystals is used as UV nonlinear optical (NLO) crystals for laser frequency conversion by the second harmonic genetation (SHG).[3−5] β-BaB_2O_4 (BBO)[6] with the anionic groups $[B_3O_6]^{3-}$, LiB_3O_5 (LBO),[7] CsB_3O_5 (CBO),[8] and $CsLiB_6O_{10}$ (CLBO)[9] with $[B_3O_7]^{5-}$ are a few examples.

Borate frameworks and building blocks are usually constructed using planar $[BO_3]$ triangles and tetrahedral $[BO_4]$ polyhedra. The substitution of a deep UV transparent structural unit $[BeO_4]$ for $[BO_4]$ may potentially result in new NLO-active beryllium borate anionic groups or various types of framework connections, which may promote further discovery of novel UV optical materials. Based on a theoretical study, Li[10] has proposed that beryllium borates possess the largest energy gap among all alkaline and alkaline earth borates, hence, the shortest transmission cutoff wavelength in the UV region. Typical examples of beryllium borate frameworks are the two-dimensional (2D) $[Be_2BO_3F_2]_\infty$ layers that can be found in $ABe_2BO_3F_2$ (A = Na, K, Rb, Cs, and Tl)[11−17] and 2D $[Be_3B_3O_6]_\infty$ layers that can be found in $M_2Be_2B_2O_7$ (M = Sr and Ba).[18,19] Up to now, KBe_2BO_3F is the leading deep UV NLO crystal. Because of the high toxicity of the BeO used as starting material during preparation, only a few of alkaline and alkaline earth beryllium borate compounds are reported, namely, $CaBeB_2O_5$,[20] $SrBeB_2O_5$,[21] $Sr_3BeB_6O_{13}$,[22] $SrBe_2B_2O_6$,[23] $BaBe_2B_2O_6$,[24] $Li_{14}Be_5B(BO_3)_9$,[25] $RbBe_4B_3O_9$,[26] and $CsBe_4B_3O_9$.[27] All of them have been found to crystallize in centrosymmetric space groups.

In our previous study, we reported the discovery of two kinds of beryllium borate anionic group $[BeB_2O_7]^{6-}$ and $[Be_2B_3O_{11}]^{9-}$, in which the former make up the structure of $Na_2BeB_2O_5$,[28] while the latter make up the structure of $NaBeB_3O_6$ and α-$KBe_2B_3O_7$[29] and four UV NLO crystals that include β-$KBe_2B_3O_7$, γ-$KBe_2B_3O_7$ $RbBe_2B_3O_7$,[29] and $Na_2CsBe_6B_5O_{15}$,[30] which consist of 2D $[Be_2BO_5]_\infty$ layers connected by strong covalent bonds. This approach to beryllium borate anionic group construction and various types of framework connection was successful and will allow further advances in UV optical materials exploration.

In this study, we carried out a systematic synthesis based on the $Li_2O-BeO-B_2O_3$ quasi-ternary system in order to obtain UV optical crystals containing new anionic groups or framework connection. This has led to a series of new alkaline beryllium borates with the stoichiometry $LiBeBO_3$,

Received: January 13, 2014
Published: February 17, 2014

   dx.doi.org/10.1021/ic5000843 | Inorg. Chem. 2014, 53, 2742−2748

Table 1. Crystal Data and Structure Refinement for $LiBeBO_3$, $Li_6Be_3B_4O_{12}$, and $Li_8Be_5B_6O_{18}$

formula	$LiBeBO_3$	$Li_6Be_3B_4O_{12}$	$Li_8Be_5B_6O_{18}$
formula mass(amu)	74.76	303.91	453.43
crystal system	Triclinic	Triclinic	Triclinic
space group	*P*-1	*P*-1	*P*-1
a (Å)	4.626(3)	4.6677(16)	4.698(3)
b (Å)	4.686(3)	9.025(3)	11.565(8)
c (Å)	5.894(5)	11.344(5)	11.870(8)
α (°)	68.22(5)	105.072(17)	77.849(13)
β (°)	72.01(5)	101.436(14)	89.420(18)
γ (°)	61.02(4)	103.521(15)	89.210(16)
V (Å^3)	102.47(14)	431.2(3)	630.3(7)
Z	2	2	2
crystal size (mm)	0.35 × 0.3 × 0.03	0.7 × 0.15 × 0.15	0.5 × 0.1 × 0.05
ρ (calcd)(g/cm^3)	2.423	2.34	2.389
temperature (K)	293(2)	293(2)	293(2)
λ (Å)	0.71073	0.71073	0.71073
F (000)	72	292	436
μ (mm^{-1})	0.215	0.205	0.21
θ (deg)	3.77−27.47	2.45−27.47	2.24−27.51
index range	$-5 \le h \le 5$	$-6 \le h \le 6$	$-6 \le h \le 6$
	$-6 \le k \le 6$	$-11 \le k \le 11$	$-15 \le k \le 15$
	$-7 \le l \le 7$	$-14 \le l \le 14$	$-15 \le l \le 15$
R_{int}	0.0164	0.0126	0.0393
reflections collected	778	3313	4909
reflections (I > 2σ(I))/ independent reflections	375/434	1623/1734	2094/2688
data/restraints/parameters	434/0/55	1734/0/227	2688/0/334
R/w*R*[a] (I > 2σ (I))	0.0311/0.0739	0.0244/0.0648	0.0563/0.1637
R/w*R* (all data)	0.0375/0.081	0.0263/0.0661	0.0711/0.1729
GOF on F^2	1.067	1.109	1.209
largest diff. peak and hole (e/Å^{-3})	0.226 and −0.27	0.239 and −0.283	0.451 and −0.386

[a] $R(F) = \Sigma||F_o| - |F_c||/\Sigma|F_o|$. $wR(F_o^2) = [\Sigma w(F_o^2 - F_c^2)^2/\Sigma w(F_o^2)^2]^{1/2}$.

$Li_6Be_3B_4O_{12}$, and $Li_8Be_5B_6O_{18}$. The phase diagrams, crystal growth, structures, thermal behavior, and spectra of these borates are reported in this paper.

EXPERIMENTAL SECTION

Reagents. Li_2CO_3 (99.8%), BeO (99.5%), and B_2O_3 (99.5%) were purchased from Sinopharm and used as received.

Phase Equilibria in Li_2O−BeO−B_2O_3 System and Crystal Growth. Phase equilibria in the Li_2O−BeO−B_2O_3 system were investigated using the method of visual polythermal analysis (VPA),[31,32] spontaneous crystallization from the melt, and X-ray diffraction (XRD). The VPA method makes it possible to determine the crystallization temperature in a high-temperature solution with specified composition and to construct the liquid line. The high temperature solution was prepared by melting a mixture of Li_2CO_3, BeO, and B_2O_3 at different molar ratios in a platinum crucible. The mixture (10 g) was heated in a precise programmable temperature electric furnace with a thermal field of high symmetry and stability (±0.1 °C) at 1050 °C until the melt became transparent and clear. The homogenized melt solution was cooled rapidly to 1000 °C. Then the furnace temperature was decreased stepwise by 5 °C increments; in each temperature stage, the solution was kept for 4−6 h before the melt surface was observed. Once the onset of crystallization was visually observed, the melt was slowly cooled at a rate of 3 °C/h for 5 h, and finally to room temperature after the furnace was turned off. The flux attached to the crystal was readily dissolved in water and the crystals that contained no inclusions were examined by powder XRD. Single crystals of $LiBeBO_3$, $Li_6Be_3B_4O_{12}$, and $Li_8Be_5B_6O_{18}$ were obtained within the specified range (discussed below). This technique makes it possible to effectively eliminate the melt undercooling and accurately determine the temperature of primary crystal formation within ±5 °C accuracy.

Single Crystal X-ray Diffraction. Single XRD data were collected at room temperature on a Rigaku Mercury CCD diffractometer with graphite-monochromatic Mo Kα radiation (λ = 0.71073 Å). A transparent block of crystal was mounted on a glass fiber with epoxy for structure determination. A hemisphere of data was collected using a narrow-frame method with the ω-scan mode. The data were integrated using the CrystalClear program, and the intensities were corrected for Lorentz polarization, air absorption, and absorption attributable to the variation in the path length through the detector faceplate. Absorption corrections based on the Multiscan technique were also applied. The structure was solved by direct methods using SHELXS-97 and then refined by full-matrix least-squares refinement on F^2 with SHELXL-97[33] found in the software suite WinGX[34] v 1.80.05. All of the structures were verified using ADDSYM algorithm from the program PLATON,[35] and no higher symmetries were found. Relevant crystallographic data and details of the experimental conditions for $LiBeBO_3$, $Li_6Be_3B_4O_{12}$, and $Li_8Be_5B_6O_{18}$ are summarized in Table 1. Atomic coordinates, isotropic displacement coefficients, and BVS are listed in Table S1−S3 in the Supporting Information.

Powder X-ray Diffraction. X-ray diffraction patterns of polycrystalline materials were obtained on a Rigaku D_{max}2500 diffractometer by using Cu Kα radiation (λ = 1.540598 Å) at room temperature in the angular range of 2θ = 0−60° with a scan step width of 0.05° and a fixed time of 0.2 s.

Elemental Analysis. Elemental analysis of the crystals was performed by using a Jobin Yvon Ultima2 inductively coupled plasma optical emission spectrometer (ICP-OES) with Sepex Certiprep standards. The crystal samples were dissolved in a mixture of nitric acid (3 mL) and hydrochloric acid (3 mL).

Differential Thermal Analysis. Differential thermal analysis (DTA) scans were measured on a NETZSCH STA 449C

dx.doi.org/10.1021/ic5000843 | Inorg. Chem. 2014, 53, 2742−2748

simultaneous analyzer. Reference (Al_2O_3) and crystal samples (5−15 mg) were enclosed in Al_2O_3 crucibles and heated from room temperature to 1200 °C at a rate of 15 °C/min under a constant flow of nitrogen gas. The DTA residues were visually inspected and then analyzed by powder XRD after the experiments.

UV−vis Diffuse Reflectance Spectroscopy. The UV−vis diffuse reflection spectra were recorded at room temperature using a powder sample with $BaSO_4$ as a standard (100% reflectance) on a PerkinElmer Lamda-900 UV/vis/NIR Spectrophotometer over the spectra range 200−800 nm. Reflectance spectra were converted to absorbance using the Kubelka−Munk function.[36,37]

RESULTS AND DISCUSSION

Phase Equilibria and Crystal Growth. In order to avoid the melt undercooling and determine the primary crystalline phase, each crystal phase was grown at a fixed temperature followed by a transient cooling process after precipitation of the desired crystallization phase instead of slow cooling to avoid glass formation and phase transitions that can occur during a slow cooling process. As a result, investigation of the Li_2O−BeO−B_2O_3 system by VPA and XRD showed the stability region for each single phase and the projection of liquid line that are displayed in a quasi-ternary phase diagram (Figure 1)

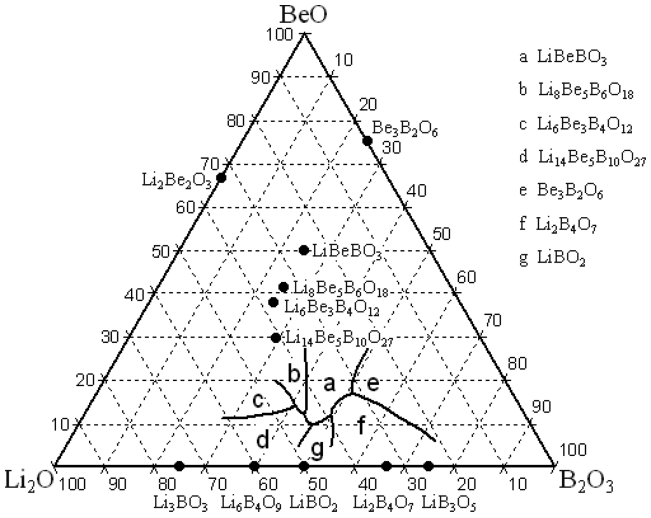

Figure 1. Primary crystallization region in the quasi-ternary phase diagram Li_2O−BeO−B_2O_3.

with the three end members BeO, Li_2O, and B_2O_3. According to available literature data, eight stoichiometric compounds exist in the Li_2O−B_2O_3[38,39] phase diagram. Only five of these compounds are stable at room temperature, namely, Li_3BO_3, $Li_6B_4O_9$, $LiBO_2$, $Li_2B_4O_7$, and LiB_3O_5. In Li_2O−BeO[40] and BeO−B_2O_3[41] systems, two compounds are known, namely, $Li_2Be_2O_3$ and $Be_2B_3O_6$, respectively. Due to the high melting point, BeO is very hard to dissolve in the Li_2O−B_2O_3 solvent below 1100 °C, except region a−g in the phase diagram. Three new ternary phases $LiBeBO_3$, $Li_6Be_3B_4O_{12}$, and $Li_8Be_5B_6O_{18}$ were found inside the triangle proven on the basis of the single crystal structure refinement besides $Li_{14}Be_5B(BO_3)_9$ found in 1994. Phase boundaries determined from powder XRD patterns are indicated in the diagram as well.

Thermal Behavior. As shown in Figure 2, the DTA curves for $LiBeBO_3$, $Li_6Be_3B_4O_{12}$, and $Li_8Be_5B_6O_{18}$ exhibit only one endothermic peak beginning at 826 °C ($LiBeBO_3$), 830 °C ($Li_6Be_3B_4O_{12}$), and 824 °C ($Li_8Be_5B_6O_{18}$) upon heating to 1200 °C, respectively. Obviously, the decomposition temperatures of these compounds were very close to that of $Li_{14}Be_5B(BO_3)_9$ (828 °C). In order to determine relationships among these four phases, long-term annealing experiments were performed. The powders of $LiBeBO_3$, $Li_6Be_3B_4O_{12}$, $Li_8Be_5B_6O_{18}$, and $Li_{14}Be_5B(BO_3)_9$ crystals were annealed at 700, 750, 775, 800, and 830 °C for 24 h, respectively, and subsequently quenched by ice. Phase analysis of the residues of these compounds was performed based on powder XRD pattern. It revealed that both $LiBeBO_3$ and $Li_{14}Be_5B(BO_3)_9$ were thermally stable up to about 830 °C and then decomposed into BeO above 830 °C, whereas $Li_6Be_3B_4O_{12}$ and $Li_8Be_5B_6O_{18}$ were decomposed in the temperature range of 700−750 °C into $Li_{14}Be_5B(BO_3)_9$ and BeO, $Li_{14}Be_5B(BO_3)_9$, $LiBeBO_3$, and BeO, respectively. The transition of these phases is shown in Figure 3. Hence, $LiBeBO_3$ and $Li_{14}Be_5B(BO_3)_9$ exhibit higher thermally stability than $Li_6Be_3B_4O_{12}$ and $Li_8Be_5B_6O_{18}$, and the endothermic peak located at 826 and 830 °C on the DTA curves for $LiBeBO_3$ and $Li_6Be_3B_4O_{12}$ should be attributed to the thermal decomposition of $LiBeBO_3$ and $Li_{14}Be_5B(BO_3)_9$, repectively, whereas the endothermic peak located at 824 °C on the DTA curves for $Li_8Be_5B_6O_{18}$ represent the thermal decomposition of the mixture of $LiBeBO_3$ and $Li_{14}Be_5B(BO_3)_9$. No obvious thermal peaks were observed on the DTA curves of $Li_6Be_3B_4O_{12}$ and

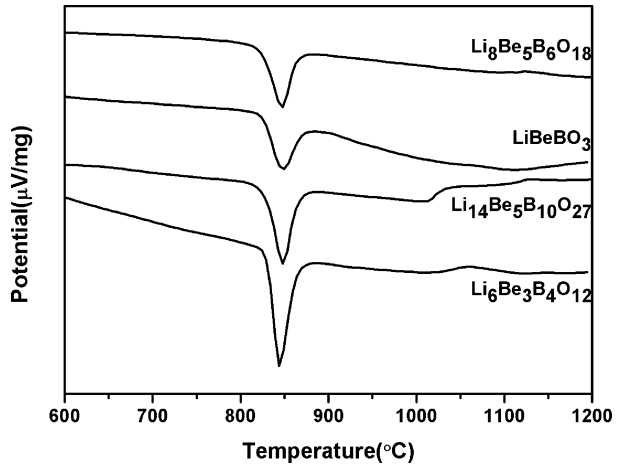

Figure 2. DTA trace for the compositions of $LiBeBO_3$, $Li_6Be_3B_4O_{12}$, $Li_8Be_5B_6O_{18}$, and $Li_{14}Be_5B(BO_3)_9$.

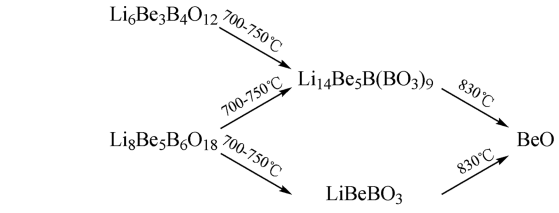

$Li_6Be_3B_4O_{12}$ —700-750℃→ $Li_{14}Be_5B(BO_3)_9$ + BeO + Liquid

$Li_8Be_5B_6O_{18}$ —700-750℃→ $Li_{14}Be_5B(BO_3)_9$ + $LiBeBO_3$ + BeO + Liquid

$Li_{14}Be_5B(BO_3)_9$ —830℃→ BeO + Liquid

$LiBeBO_3$ —830℃→ BeO + Liquid

Figure 3. Transition of $LiBeBO_3$, $Li_6Be_3B_4O_{12}$, $Li_8Be_5B_6O_{18}$, and $Li_{14}Be_5B(BO_3)_9$.

dx.doi.org/10.1021/ic5000843 | Inorg. Chem. 2014, 53, 2742−2748

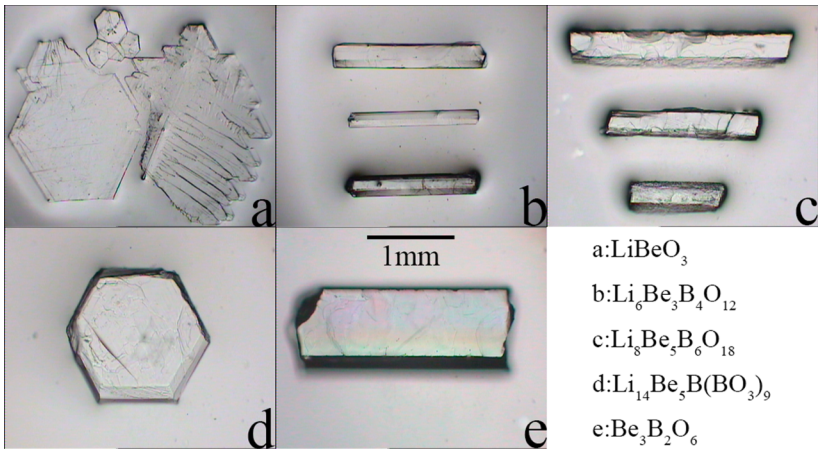

Figure 4. Crystal pictures: (a) $LiBeBO_3$, (b) $Li_6Be_3B_4O_{12}$, (c) $Li_8Be_5B_6O_{18}$, (d) $Li_{14}Be_5B(BO_3)_9$, and (e) $Be_3B_2O_6$.

$Li_8Be_5B_6O_{18}$ that would correspond to the aforementioned phase transitions, which were expected to occur below 830 °C.

Based on their incongruent melting behavior, transparent and colorless $LiBeBO_3$, $Li_6Be_3B_4O_{12}$, $Li_8Be_5B_6O_{18}$, and $Be_2B_3O_6$[41] crystals have been grown by spontaneous crystallization in a molten flux based on the self-fluxed system Li_2O–B_2O_3. They are all chemically stable in the water. Crystal pictures of $LiBeBO_3$, $Li_6Be_3B_4O_{12}$, $Li_8Be_5B_6O_{18}$, $Li_{14}Be_5B(BO_3)_9$, and $Be_3B_2O_6$ are shown in Figure 4.

Crystal Structure. $LiBeBO_3$, $Li_6Be_3B_4O_{12}$, and $Li_8Be_5B_6O_{18}$ crystallize in the same centrosymmetric triclinic space group *P*-1. In these structures, all the B atoms are coordinated to three O atoms to form planar $[BO_3]$ triangles and all the Be atoms are bound to four O atoms to form distorted $[BeO_4]$ tetrahedral.

$LiBeBO_3$. The structure is illustrated along the *c*-axis in Figure 5. In this structure, B–O and Be–O bond lengths range from

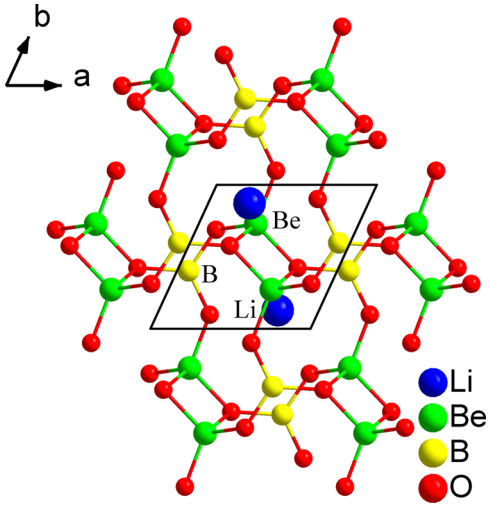

Figure 5. Crystal structure of $LiBeBO_3$.

1.355(2) to 1.404(2) Å and 1.571(3) to 1.739(3) Å, while O–B–O and O–Be–O bond angles range from 118.58(16) to 121.04(16)° and 91.90(13) to 115.63(15)°, respectively. All O atoms are twofold coordinated except O3, which is threefold coordinated. In the $LiBeBO_3$ structure, two $[BeO_4]$ tetrahedra share an edge to form a $[Be_2O_6]$ dimer which has a nearly square four-membered-ring $[Be_2O_2]$. The adjacent $[Be_2O_6]$ building blocks are connected via sharing vertexes with $[BO_3]$ triangles to form infinite layers in the *a*–*b* plane. The adjacent layers are separated by planes of Li cations which are in a 4 coordination environment with Li–O bond lengths ranging from 1.875(3) to 2.049(3) Å.

$Li_6Be_3B_4O_{12}$. The structure is illustrated in Figure 6. In this structure, B–O and Be–O bond lengths range from

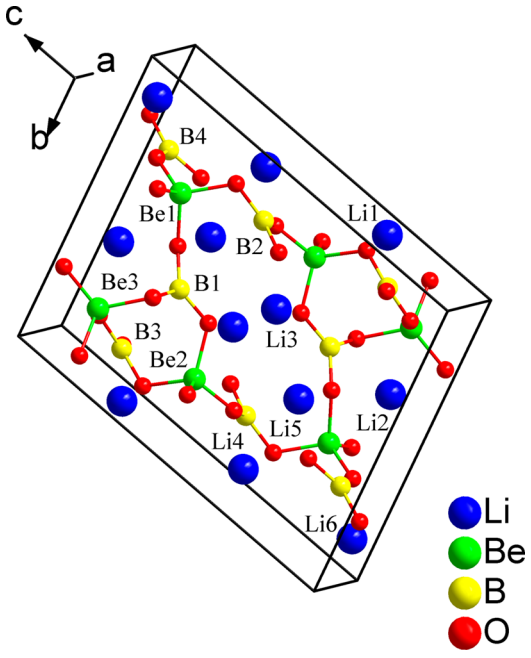

Figure 6. Crystal structure of $Li_6Be_3B_4O_{12}$.

1.3711(13) to 1.3878(15) Å and 1.6157(15) to 1.6793(15) Å, while O–B–O and O–Be–O bond angles range from 118.63(9) to 122.01(10)° and 103.57(8) to 114.27(9)°, respectively. All O atoms are twofold coordinated. In the $Li_6Be_3B_4O_{12}$ structure, four $[BeO_4]$ tetrahedra (2 × Be1 and 2 × Be2) and four $[BO_3]$ triangles (2 × B1 and 2 × B2) share vertexes successively to form a 16-membered-ring $[Be_4B_4O_{20}]$. Then other $[BeO_4]$ tetrahedra (2 × Be3) and $[BO_3]$ triangles (2 × B3) ouside the ring are connected to the $[BeO_4]$ tetrahedra (2 × Be2) and $[BO_3]$ triangles (2 × B1) of the ring via vertex-sharing to form two 8-membered-ring $[Be_2B_2O_{10}]$ on both sides of the $[Be_4B_4O_{20}]$ ring, which looks like a pair of

dx.doi.org/10.1021/ic5000843 | Inorg. Chem. 2014, 53, 2742–2748

wings of the "plane". Additional [BO_3] triangles (2 × B4) are connected to the [BeO_4] tetrahedra (2 × Be1) of the 16-membered-ring by sharing vertexes. The "plane" and the two [BO_3] triangles (2 × B4) constitute fundamental building block (FBB) of $Li_6Be_3B_4O_{12}$, which can be written as [$Be_6B_8O_{32}$]. The adjacent [$Be_6B_8O_{32}$] FBB are connected via sharing their peripheral O atoms to form infinite layers along the $a-c$ plane. In other words, each [BeO_4] tetrahedron is surrounded by four [BO_3] triangles and each [BO_3] triangle is surrounded by three [BeO_4] tetrahedra in this structure. The adjacent layers are separated by Li^+ cations. The Li^+ cations reside in these cages, where Li1−Li6 cations are all located in a 4 coordination environment with Li−O bond lengths ranging 1.9054(19)−1.979(2) Å, 1.928(2)−2.275(3) Å, 1.9047(19)−2.0527(19) Å, 1.9271(19)−2.045(2) Å, 1.889(2)−2.076(2) Å, and 1.906(2)−2.135(2) Å, respectively.

$Li_8Be_5B_6O_{18}$. The structure is shown in Figure 7. In this structure, B−O and Be−O bond lengths range from 1.347(4)

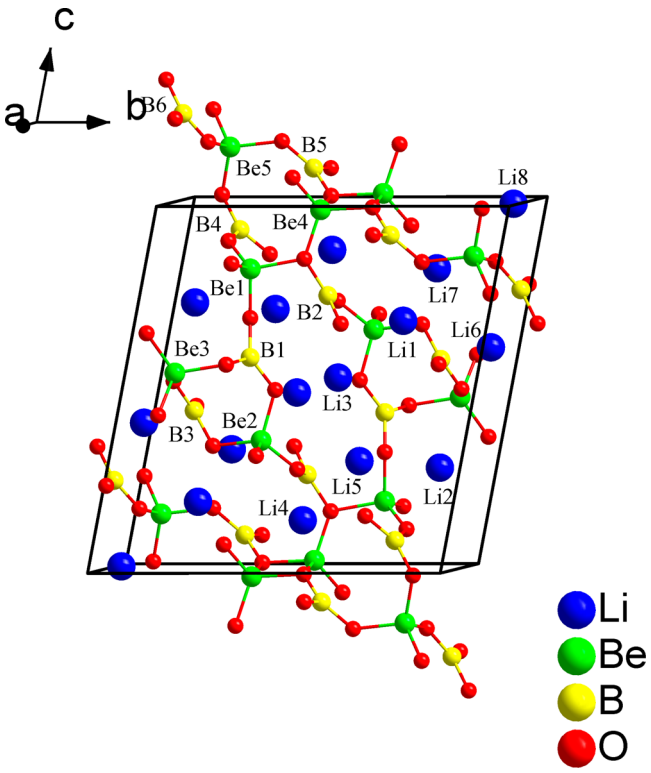

Figure 7. Crystal structure of $Li_8Be_5B_6O_{18}$.

to 1.419(4) Å and 1.561(4) to 1.747(5) Å, while O−B−O and O−Be−O bond angles range from 117.2(3) to 122.7(3)° and 91.2(2) to 115.8(3)°, respectively. All O atoms are twofold coordinated except O5 and O13, which are threefold coordinated. A similar structure unit of [$Be_6B_8O_{32}$] to that in $Li_6Be_3B_4O_{12}$ was found in $Li_8Be_5B_6O_{18}$. In this structure, two [BeO_4] tetrahedral (2 × Be4) share an edge to form a [Be_2O_6] dimer, and then connect to four [BO_3] triangles (2 × B5 and 2 × B6) and two [BeO_4] tetrahedral (2 × Be5) on both sides of the dimer by sharing vertexes to form a [$Be_4B_4O_{20}$] chain. The [$Be_6B_8O_{32}$] structure units are connected by sharing the O atoms with the [$Be_4B_4O_{20}$] chain to constitute the FBB of $Li_8Be_5B_6O_{18}$, which can be written as [$Be_{10}B_{12}O_{50}$]. The adjacent [$Be_{10}B_{12}O_{50}$] FBB are connected via sharing their peripheral O atoms to form infinite layers along the $b-c$ plane, resulting in the final 3D open framework with cages. The Li^+ cations reside in these cages, where Li1, Li3, Li5, Li6, Li7, and Li8 cations are all located in a 4-coordination environment with Li−O bond lengths ranging 1.914(6)−2.007(7) Å, 1.885(7)−2.047(7) Å, 1.870(7)−2.131(7) Å, 1.869(7)−2.154(8) Å, 1.890(7)−2.003(7) Å, and 1.899(6)−2.049(7) Å, respectively; Li2 and Li4 cations are located in a 4 + 1 coordination environment with one considerably longer Li−O bond of 2.650(9) Å and 2.666(7) Å, respectively. Although $LiBeBO_3$, $Li_6Be_3B_4O_{12}$, and $Li_8Be_5B_6O_{18}$ contain NLO-active [BO_3] groups, their centrosymmetric alignment results in the cancellation of NLO susceptibilities.

It is worth comparing the structure of $LiBeBO_3$, $Li_6Be_3B_4O_{12}$, and $Li_8Be_5B_6O_{18}$ because of the structural similarity. The difference in structures among them can be clearly distinguished by their FBB as shown in Figure 8. The FBB [$Be_6B_8O_{32}$] of $Li_6Be_3B_4O_{12}$, FBB [$Be_2B_2O_{10}$] of $LiBeBO_3$, and two other structure units [$BeBO_6$] constitute the FBB [$Be_{10}B_{12}O_{50}$] of $Li_8Be_5B_6O_{18}$, which is consistent with the summation of the stoichiometry $Li_6Be_3B_4O_{12}$ + $LiBeBO_3$ + $LiBeBO_3$ = $Li_8Be_5B_6O_{18}$.

Although the compound $Be_3B_2O_6$[41] was reported in 1965, the crystal structure has not been determined. In our experiments, a lot of $Be_3B_2O_6$ crystals went evaluated by single XRD measurement, but the structure problem has not been solved yet.

Figure S1 (Supporting Information) shows the powder XRD patterns for grown crystals of $LiBeBO_3$, $Li_6Be_3B_4O_{12}$, $Li_8Be_5B_6O_{18}$, and $Li_{14}Be_5B(BO_3)_9$. The peak positions match the theoretical patterns simulated from single crystal refinement. The powder XRD patterns of $Be_3B_2O_6$ are also shown in Figure S1.

The results of ICP elemental analysis of $LiBeBO_3$, $Li_6Be_3B_4O_{12}$, and $Li_8Be_5B_6O_{18}$ (Table 2) were consistent with the compositions determined from single crystal refinement. The results of ICP elemental analysis of $Be_3B_2O_6$ were consistent with the compositions reported previously.

Optical Properties. UV−vis diffuse reflectance spectra were collected for all of the reported compounds (see Figure S2 in the Supporting Information). Absorption (K/S) data were calculated from the following Kubelka−Munk function:[36,37] $F(R) = (1 - R)^2/2R = K/S$, where R is the reflectance, K is the absorption, and S is the scattering. No obvious absorption peak in the range of 6.22−1.55 eV (corresponding to 200−800 nm) was observed for $LiBeBO_3$, $Li_6Be_3B_4O_{12}$, and $Li_8Be_5B_6O_{18}$, indicating that these crystals may be suitable for deep UV applications.

CONCLUSIONS

Phase formation in the $Li_2O-BeO-B_2O_3$ system was investigated by the methods of visual polythermal analysis, spontaneous crystallization, and XRD. Three new alkaline beryllium borates $LiBeBO_3$, $Li_6Be_3B_4O_{12}$, and $Li_8Be_5B_6O_{18}$ have been synthesized by spontaneous crystallization with molten flux based on $Li_2O-B_2O_3$ solvent in this system. The similarity of the fundamental building blocks of the title compounds has been compared. The UV−vis diffuse reflectance spectroscopy indicated that the UV cutoff edges of these centrosymmetric compounds are all below 200 nm. Our further research efforts will be devoted to the explorations of other new UV materials.

dx.doi.org/10.1021/ic5000843 | Inorg. Chem. 2014, 53, 2742−2748

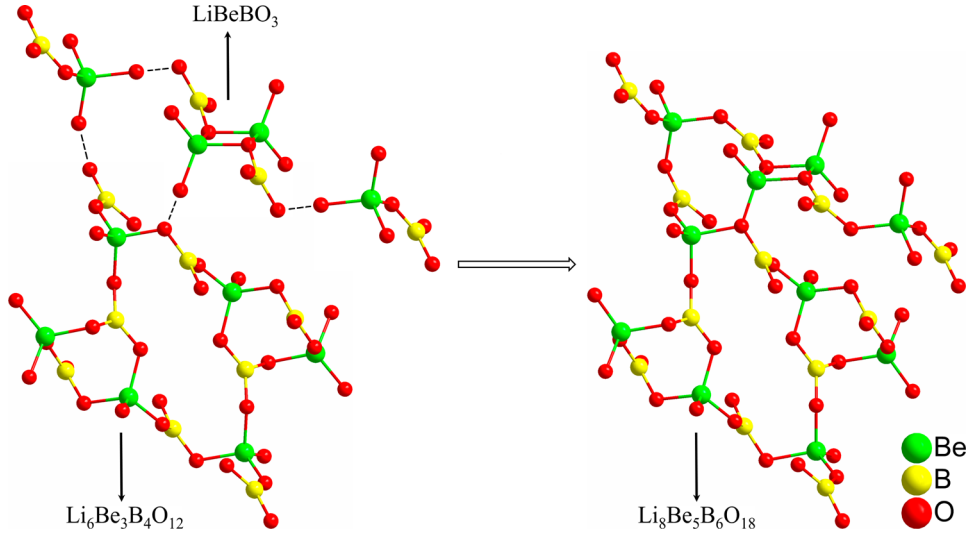

Figure 8. Relationship of the fundamental building block among $LiBeBO_3$, $Li_6Be_3B_4O_{12}$, and $Li_8Be_5B_6O_{18}$.

Table 2. ICP Elemental Analysis and Stoichiometry for $LiBeBO_3$, $Li_6Be_3B_4O_{12}$, $Li_8Be_5B_6O_{18}$, and $Be_3B_2O_6$

	Li	Be	B
$LiBeBO_3$	1.01	0.98	1
$Li_6Be_3B_4O_{12}$	6	3.08	3.76
$Li_8Be_5B_6O_{18}$	8.02	5	5.78
$Be_3B_2O_6$	-	3	2.15

■ ASSOCIATED CONTENT

Supporting Information

Atomic positions, powder XRD patterns, diffuse reflectance absorption curves, and crystal data (CIF). This material is available free of charge via the Internet at http://pubs.acs.org.

■ AUTHOR INFORMATION

Corresponding Author

*E-mail: nye@fjirsm.ac.cn.

Notes

The authors declare no competing financial interest.

■ ACKNOWLEDGMENTS

This research was supported by the National Natural Science Foundation of China (Nos. 91222204 and 90922035), Main Direction Program of Knowledge Innovation of Chinese Academy of Sciences (Grant No. KJCX2-EW-H03-03), and Special Project of National Major Scientific Equipment Development of China (No. 2012YQ120060).

■ REFERENCES

(1) Gerasimova, N. G. *Instrum. Exp. Tech.* **2006**, *49*, 408−412.
(2) Zhou, G. Q.; Xu, J.; Chen, X. D.; Zhong, H. Y.; Wang, S. T.; Xu, K.; Deng, P. Z.; Gan, F. X. *J. Cryst. Growth* **1998**, *191*, 517−519.
(3) Yu, H. W.; Wu, H. P.; Pan, S. L.; Yang, Z. H.; Su, X.; Zhang, F. F. *J. Mater. Chem.* **2012**, *22*, 9665−9670.
(4) Wu, H. P.; Yu, H. W.; Pan, S. L.; Huang, Z. J.; Yang, Z. H.; Su, X.; Poeppelmeier, K. R. *Angew. Chem., Int. Ed.* **2013**, *52*, 3406−3410.
(5) Wu, H. P.; Yu, H. W.; Yang, Z. H.; Hou, X. L.; Su, X.; Pan, S. L.; Poeppelmeier, K. R.; Rondinelli, J. M. *J. Am. Chem. Soc.* **2013**, *135*, 4215−4218.
(6) Chen, C. T.; Wu, B. C.; Jiang, A. D.; You, G. M. *Scientia Sinica Series B-Chemical Biological Agricultural Medical & Earth Sciences* **1985**, *28*, 235−243.
(7) Chen, C. T.; Wu, Y. C.; Jiang, A. D.; Wu, B. C.; You, G. M.; Li, R. K.; Lin, S. J. *J. Opt. Soc. Am. B* **1989**, *6*, 616−621.
(8) Wu, Y. C.; Sasaki, T.; Nakai, S.; Yokotani, A.; Tang, H. G.; Chen, C. T. *Appl. Phys. Lett.* **1993**, *62*, 2614−2615.
(9) Mori, Y.; Kuroda, I.; Nakajima, S.; Sasaki, T.; Nakai, S. *Appl. Phys. Lett.* **1995**, *67*, 1818−1820.
(10) Li, R. K. *J. Non-Cryst. Solids* **1989**, *111*, 199−204.
(11) Chen, C. T.; Wang, G. L.; Wang, X. Y.; Xu, Z. Y. *Appl. Phys. B* **2009**, *97*, 9−25.
(12) Mei, L. F.; Wang, Y. B.; Chen, C. T. *Mater. Res. Bull.* **1994**, *29*, 81−87.
(13) Mei, L.; Huang, X.; Wang, Y.; Wu, Q.; Wu, B.; Chen, C. *Z. Kristallogr.* **1995**, *210*, 93−95.
(14) McMillen, C. D.; Kolis, J. W. *J. Cryst. Growth* **2008**, *310*, 2033−2038.
(15) Chen, C. T.; Luo, S. Y.; Wang, X. Y.; Wang, G. L.; Wen, X. H.; Wu, H. X.; Zhang, X.; Xu, Z. Y. *J. Opt. Soc. Am. B* **2009**, *26*, 1519−1525.
(16) McMillen, C. D.; Hu, J.; VanDerveer, D.; Kolis, J. W. *Acta Crystallogr., Sect. B* **2009**, *65*, 445−449.
(17) Huang, H. W.; Chen, C. T.; Wang, X. Y.; Zhu, Y.; Wang, G. L.; Zhang, X.; Wang, L. R.; Yao, J. Y. *J. Opt. Soc. Am. B* **2011**, *28*, 2186−2190.
(18) Chen, C. T.; Wang, Y. B.; Wu, B. C.; Wu, K. C.; Zeng, W. L.; Yu, L. H. *Nature* **1995**, *373*, 322−324.
(19) Qi, H.; Chen, C. T. *Chem. Lett.* **2001**, 352−353.
(20) Schaffers, K. I.; Keszler, D. A. *Acta Crystallogr., Sect. C* **1993**, *49*, 647−650.
(21) Yao, W.; Wang, X.; Huang, H.; Xu, T.; Jiang, X.; Wang, X.; Lin, Z.; Chen, C. *J. Alloys Compd.* **2014**, *593*, 256−260.
(22) Yao, W. J.; Huang, H. W.; Yao, J. Y.; Xu, T.; Jiang, X. X.; Lin, Z. S.; Chen, C. T. *Inorg. Chem.* **2013**, *52*, 6136−6141.
(23) Schaffers, K. I.; Keszler, D. A. *J. Solid State Chem.* **1990**, *85*, 270−274.
(24) Schaffers, K. I.; Keszler, D. A. *Inorg. Chem.* **1994**, *33*, 1201−1204.
(25) Luce, J. L.; Schaffers, K. I.; Keszler, D. A. *Inorg. Chem.* **1994**, *33*, 2453−2455.
(26) Wen, X. H.; Li, R. K.; Chen, C. T. *Acta Crystallogr., Sect. C* **2006**, *62*, I21−I23.
(27) Huang, H. W.; Yao, W. J.; He, R.; Chen, C. T.; Wang, X. Y.; Zhang, Y. H. *Solid State Sci.* **2013**, *18*, 105−109.
(28) Li, W.; Ye, N. *Acta Crystallogr., Sect. E.* **2007**, *63*, I160−U71.
(29) Wang, S. C.; Ye, N.; Li, W.; Zhao, D. *J. Am. Chem. Soc.* **2010**, *132*, 8779−8786.
(30) Wang, S. C.; Ye, N. *J. Am. Chem. Soc.* **2011**, *133*, 11458−11461.

(31) Bekker, T. B.; Kokh, A. E.; Kononova, N. G.; Fedorov, P. P.; Kuznetsov, S. V. *Cryst. Growth Des.* **2009**, *9*, 4060−4063.
(32) Bekker, T. B.; Fedorov, P. P.; Kokh, A. E. *Cryst. Growth Des.* **2012**, *12*, 129−134.
(33) Sheldrick, G. M. *Acta Crystallogr., Sect. A* **2008**, *64*, 112−122.
(34) Farrugia, L. J. *J. Appl. Crystallogr.* **1999**, *32*, 827−838.
(35) Spek, A. L. *J. Appl. Crystallogr.* **2003**, *36*, 7−13.
(36) Kubelka, P.; Munk, F. *Z. Tech. Phys* **1931**, *12*, 593−601.
(37) Tauc, J. *Mater. Res. Bull.* **1970**, *5*, 721−&.
(38) Sastry, B. S. R.; Hummel, F. A. *J. Am. Ceram. Soc.* **1958**, *41*, 7−17.
(39) Sastry, B. S. R.; Hummel, F. A. *J. Am. Ceram. Soc.* **1959**, *42*, 216−218.
(40) Turner, P. P.; Bartram. *Inorg. Chem.* **1967**, *6*, 833−&.
(41) Blackbur, Pe; Buchler, A. *J. Phys. Chem.* **1965**, *69*, 4250−&.

dx.doi.org/10.1021/ic5000843 | *Inorg. Chem.* 2014, 53, 2742−2748